

1 **A standardized index for assessing sub-monthly compound**
2 **dry and hot conditions: application in China**

3 Jun Li¹, Zhaoli Wang^{1,2}, Xushu Wu^{1,2,*}, Jakob Zscheischler^{3,4,5}, Shenglian Guo⁶,
4 Xiaohong Chen⁷

5 ¹ *School of Civil Engineering and Transportation, State Key Laboratory of Subtropical*
6 *Building Science, South China University of Technology, Guangzhou 510641, China.*

7 ² *Guangdong Engineering Technology Research Center of Safety and Greenization for*
8 *Water Conservancy Project, Guangzhou 510641, China.*

9 ³ *Climate and Environmental Physics, University of Bern, Sidlerstrasse 5, 3012 Bern,*
10 *Switzerland.*

11 ⁴ *Oeschger Centre for Climate Change Research, University of Bern, Bern, Switzerland.*

12 ⁵ *Department of Computational Hydrosystems, Helmholtz Centre for Environmental*
13 *Research - UFZ, Leipzig, Germany*

14 ⁶ *State Key Laboratory of Water Resources and Hydropower Engineering Science,*
15 *Wuhan University, Wuhan 430072, China.*

16 ⁷ *Center for Water Resource and Environment, Sun Yat-Sen University, Guangzhou*
17 *510275, China*

18 **Correspondence: xshwu@scut.edu.cn.*

19

20 **Abstract:** Compound dry-hot conditions pose large impacts on ecosystems and society
21 worldwide. A suite of indices are proposed for the assessments of droughts and
22 heatwaves previously, yet there is no index available for incorporating the joint
23 variability of dry and hot conditions at sub-monthly scale. Here, we introduce a daily-
24 scale index, termed as the standardized compound drought and heat index (SCDHI), to
25 measure the intensity of compound dry and hot conditions. SCDHI is based on the daily
26 drought index (the standardized antecedent precipitation evapotranspiration index
27 (SAPEI)) and the standardized temperature index (STI) and a joint probability
28 distribution method. The new index is verified against real-world compound dry and
29 hot events and the related observed vegetation impacts in China. SCDHI can not only
30 monitor the long-term compound dry and hot events, but also capture such events at
31 sub-monthly scale and reflect the related vegetation activity impacts. The identified
32 compound events generally persisted for 25-35 days and the southern China suffered
33 from compound events most frequently. In future, the frequency, duration, severity and
34 intensity of compound events increase throughout China in response to anthropogenic
35 climate change, of which the frequency would generally increase by 1-3 times and the
36 duration and severity increase by 50%; under largest emission scenario, duration,
37 severity, and frequency across Midwest China increase by at least 3 times. The new
38 index can provide a new tool to quantify sub-monthly characteristics of compound dry
39 and hot events, conducive to the timely monitoring of their initiation, development, and
40 decay which are vital for decision-makers and stake-holders to release early and timely
41 warnings.

42 **Keywords:** compound event; SCDHI; SAPEI; sub-monthly scale; China

43

44 **1 Introduction**

45 Compound dry-hot event have been observed for all continents in recent decades
46 (Hao et al., 2019; Mazdiyasi and AghaKouchak, 2015; Manning et al., 2019; Sutanto
47 et al., 2020). The frequent compound dry-hot events have led to more devastating
48 impacts on natural ecosystems and human society than individual events (Zscheischler
49 et al., 2014, 2018; Chen et al., 2019; Hao et al., 2018a). Unfortunately, the extreme
50 droughts and hots are expected to occur more frequently in the coming decades under
51 global warming, which potentially results in more compound events in many parts of
52 the world, especially for wet and humid regions (Wu et al., 2020; Swain et al., 2018,
53 Zscheischler and Seneviratne, 2017a). Therefore, understanding such events are of
54 crucial importance to provide the most fundamental information to help disaster
55 mitigation.

56 Much effort has been made to study the compound events in recent years. Utilizing
57 different thresholds to define the concurrent climate extremes for a specific period, the
58 frequency of compound events has received a great deal of attention (Wu et al., 2019;
59 Zhang et al., 2019). Although this approach can detect compound event occurrence, it
60 fails to quantitatively measure compound event characteristics such as duration,
61 severity, and intensity, and is inconvenient for comparison of compound event
62 characteristics through different climates (Wu et al., 2020). Therefore, to overcome
63 these shortages, several joint climate extreme indices have been proposed for analyzing
64 the characteristics of the compound events. Specifically, the standardized dry and hot
65 index based on the ratio of the marginal probability distribution functions of
66 precipitation and temperature was proposed to measure the extreme degree of a
67 compound drought and hot extreme event (Hao et al., 2018). Hao et al. (2019, 2020)
68 recently proposed the standardized compound event indicator and compound dry-hot

69 index to assess the severity of compound dry and hot events by jointing the marginal
70 distribution of standardized precipitation index (SPI) and standardized temperature
71 index (STI) using the copula theory. These two joint indices provide useful tools to
72 improve our understanding of the frequency, spatial extent and severity of the
73 compound dry-hot event. However, they are inevitably subjected to some shortcomings
74 including the fixed monthly scale and the disregard of evapotranspiration, which may
75 limit their use in monitoring the detailed evolution of compound dry and hot events.

76 With the occurrence of extreme climate (e.g. high temperature, low humidity, and
77 sunny skies), droughts can evolve rapidly (Koster et al., 2019; Otkin et al., 2018; Yuan
78 et al., 2019; Li et al., 2020a). Such extreme weather can appear within a short period
79 without resulting in long-lasting compound events, but rather, short-term droughts and
80 heatwaves lasting a few weeks or even days (Mo and Lettenmaier, 2016; Zhang et al.,
81 2019). Severe concurrent drought and heat can suddenly strike a region with a relatively
82 short duration when extreme weather anomalies persist over the same region
83 (Röthlisberger and Martius, 2019; Wang et al., 2016). Concurrent short-term drought
84 and hot can pose greater potential socio-economic risks because the combination of
85 these events can exacerbate their respective environmental and societal impacts (Kirono
86 et al., 2017; Schumacher et al., 2019; Sedlmeier et al., 2018). Specifically, even short-
87 term concurrent dry and hot extremes can lead to significant agricultural loss if they
88 occur within sensitive stages in crop development such as emergence, pollination, and
89 grain filling (Zhang et al., 2019). Under climate change, short-term concurrent dry and
90 hot extremes are expected to increase (especially for humid regions), potentially
91 causing substantial damage to natural ecosystems and society (Li et al., 2020b; Sun et
92 al., 2019). To improve understanding of such short-term compound events and make
93 early and timely warnings, decision-makers and stakeholders require more detailed

94 information such as the start time, severity, and the projected tendency in the coming
95 days rather than the average state at a fixed monthly scale. Correspondingly, sub-
96 monthly scale indices for characterizing short-term compound dry and hot events are
97 needed. In addition, through the influence of evapotranspiration, short-term
98 meteorological variables (e.g., temperature and radiation) are considered an important
99 factor in drought and heatwave concurrences (James et al., 2010). Thus, the
100 development of a compound drought and heat index should consider other important
101 drought/hot-related factors including temperature and evapotranspiration.

102 The complexity of compound events makes it an unusual task to develop a simple
103 and robust index to quantify their past and future changes (Zscheischler et al., 2020). A
104 suite of indices are proposed for the assessments of droughts and heatwaves previously,
105 yet there is no index available for incorporating the joint variability of dry and hot
106 conditions at sub-monthly scale. Here we aim to formulate a compound drought and
107 heat index, called the standardized compound drought and heat index (SCDHI), for
108 monitoring and analyzing compound dry and hot events at sub-monthly scale. To
109 achieve this aim, we combine a daily scale drought index, the standardized antecedent
110 precipitation evapotranspiration index (SAPEI), which simultaneously considers
111 precipitation and potential evapotranspiration, with a daily scale standardized
112 temperature index (STI). We investigate the characteristics such as frequency, duration,
113 severity, and intensity of compound dry-hot events during the historical (1961-2018)
114 period and project their changes in China for the future (2050-2100) under different
115 emission scenarios. This index can provide a new tool to quantify the characteristics of
116 compound dry-hot event, and can monitor the compound dry-hot event at multiple time
117 scale (e.g., daily, weekly and monthly) to provide detailed information on their
118 initiation, development, decay, and trends.

119 **2 Methods**

120 **2.1 data**

121 Daily meteorological datasets covering 1961 to 2018 were collected from 2239
122 observational stations across the non-arid region in China (Fig. 1), which include
123 precipitation, maximum air temperature, mean air temperature, minimum air
124 temperature, relative humidity, wind speed, and sunshine duration. All of these
125 meteorological data with strict quality control are available from the China
126 Meteorological Administration (<http://cdc.nmic.cn/home.do>) and the Resources and
127 Environmental Science Data Center, Chinese Academy of Sciences
128 (<http://www.resdc.cn/Default.aspx>). The observational station data were interpolated to
129 $0.25 \times 0.25^\circ$ gridded data by kriging method, as it yields higher interpolation accuracy
130 than the other commonly used methods, e.g., ordinary nearest neighbor and inverse
131 distance weighting (Liu et al., 2016). In this study, we only focus the non-arid region
132 in China, because of three reasons: (1) replenishment of water resources across Chinese
133 arid region is mainly from melted glacial or perennial frozen soil, but not from
134 precipitation; (2) meteorological observations in Chinese arid regions are too scarce to
135 conduct robust analysis (Wu et al., 2007; Xu et al., 2015); (3) from a practical
136 perspective, calculating climate extreme indices across arid region with large-scale
137 desert regions is less meaningless (Tomas-Burguera et al., 2020).

138 The two commonly used indices (i.e., monthly Palmer drought severity index (PDSI)
139 and standardized precipitation evapotranspiration index (SPEI) were employed for
140 comparison. PDSI and SPEI were computed from the same meteorological data
141 described above. The conventional PDSI was empirically derived using the
142 meteorological data of the central USA with its semi-arid climate. The portability of

143 the conventional PDSI is thus relatively poor (Liu et al., 2017). In this study, PDSI was
144 calculated according to the China national standard of classification of meteorological
145 drought with standard number of GB/T 20481-2017. The PDSI was built based on long-
146 term meteorological data of in-situ stations evenly distributed around China, hence well
147 monitor drought in China (Zhong et al., 2019a), and the detailed calculation on the
148 PDSI is shown in supplementary materials. The 0.25°-daily root zone (0 - 100 cm) soil
149 moisture dataset obtained from Community Land Model of the Global Land Data
150 Assimilation System was also used in this study. Community Land Model product does
151 not have explicit vertical levels, instead soil moisture is represented in surface (0-2cm),
152 and root zone (0-100cm). Root zone soil moisture is chosen over the surface soil
153 moisture on account of its appositeness to characterize drought, low noise relative to
154 surface soil moisture (Hunt et al., 2009; Osman et al., 2020). The dataset from 1961 to
155 2014 were downloaded from the Goddard Earth Sciences Data and Information
156 Services Center (Rodell et al., 2004). The soil moisture dataset from Community Land
157 Model can well capture dry and wet conditions in China well (Bi et al., 2016; Feng et
158 al., 2016). To avoid the effect of seasonality, the soil moisture was fitted by Gamma
159 probability distribution, and then was standardized by normal quantile transformation.
160 In addition, 8-day leaf area index of the MOD15A2H from 2003 to 2018 were collected.
161 These data were resampled to 0.25° spatial resolution, and then the Z-score was used
162 to calculate the leaf area index anomalies.

163 We further used eight global climate models from the Coupled Model
164 Intercomparison Project Phase 5 (<https://esgf.llnl.gov/>) (Taylor et al., 2012), including
165 CanESM2, CNRM-CM5, CSIRO-Mk3.6, MIROC-ESM, MPI-ESM-LR, BCC-CSM1-
166 1, IPSL-CM5A-LR, and MRI-CGCM3, were used to project the future climate
167 conditions. These global climate models exhibit good performance to simulate the key

168 features of precipitation and temperature in China (Jiang et al., 2016; Yang et al., 2019).
169 We obtained daily climate variables (i.e., precipitation, temperature, relative humidity,
170 wind speed, and shortwave and longwave radiations) for the future (2050-2100) periods
171 for the three Representative Concentration Pathways (RCPs) including RCP 2.6 (low
172 emission scenario), RCP 4.5 (moderate emission scenario) and RCP 8.5 (high emission
173 scenario). All of the global climate models' outputs were based on the first ensemble
174 member of each model, referred to as *r1i1p1* in all of the experiments. In this study, the
175 bias-corrected climate imprint method, one of the delta statistical downscaling methods,
176 was used to downscale the global climate models outputs to a spatial resolution of 0.25°
177 (Werner and Cannon, 2016). The detailed information on these global climate models
178 is shown in Table S1.

179 **2.2 Development of SCDHI**

180 The SCDHI is a compound drought and heat index based on a daily drought index
181 and the STI, which is computed in a similar fashion as the Standardized Precipitation
182 Index (Zscheischler et al., 2014). The calculation of daily STI is similar to monthly STI,
183 but for standardizing daily temperature. For example, with respect to one certain grid
184 point, the 1 January STI are computed on the 1 January temperature datasets observed
185 during 1961-2018 at each grid point. We firstly formulated a daily scale drought index,
186 i.e. the SAPEI, by considering both precipitation and potential evapotranspiration. The
187 Penman-Monteith method is used to calculate the potential evapotranspiration.
188 Afterward, the joint distribution method was employed to compute the SCDHI.

189 **2.2.1 Formulation of daily-scale drought index**

190 Li et al. (2020b) have proposed the daily-scale drought index (SAPEI) that
191 considers both precipitation and potential evapotranspiration. However, the primary
192 limitation of this index is that it has a fixed temporal scale and cannot reflect the dry

193 and wet condition at different time scales. Hence, in this study, we developed the
194 multiple time scale (i.e., 3-, 6-, 9-, and 12-month) daily drought index. Here, we
195 followed the same nomenclature proposed by Li et al. (2020b) to refer to a daily
196 standardized drought index (SAPEI) based on precipitation and potential
197 evapotranspiration. SAPEI is simple to calculate, and uses the antecedent accumulative
198 differences between precipitation and potential evapotranspiration to represent the dry
199 and wet condition of the current day. The calculation procedure is described below.

200 The Penman-Monteith method (Allen et al., 1998) was firstly used to compute
201 potential evapotranspiration. With a value for potential evapotranspiration, the daily
202 difference between precipitation and potential evapotranspiration was calculated to
203 reveal climatic water balance (precipitation minus potential evapotranspiration). To
204 reflect dry and wet conditions of the day, the antecedent water surplus or deficit (WSD)
205 was calculated through the following equations:

$$WSD = \sum_{i=1}^n (P - PET)_i \quad (1)$$

206 Where n is the number of previous days, PET represents the potential
207 evapotranspiration, and P represents precipitation.

208 The WSD values can be aggregated at different time scales, such as 3, 6, 9 months,
209 and so on. A probability distribution was used to fit the daily time series WSD. Given
210 that different probability distributions may cause differences in drought indices (Stagge
211 et al., 2015), to select the most suitable distribution, several commonly probability
212 distributions including the general extreme value, log-logistic, lognormal, Pearson III,
213 generalized Pareto, exponential, and normal distributions, should be used to fit the
214 WSD series. In the study of Li et al. (2020b), Shapiro-Wilk and Kolmogorov-Smirnov
215 test have been used applied for optimal probability distribution selection by comparing

216 the empirical probability distribution with a candidate theoretical probability
217 distribution. They suggested that the log-logistic distribution is more suitable for SAPEI.
218 Moreover, previous researches have demonstrated that the log-logistic distribution is
219 suitable for standardizing drought indices, e.g. SPEI (Vicente-Serrano et al., 2010).
220 Therefore, we chose the log-logistic distribution to compute SAPEI. Once the daily
221 WSD series were fit to a probability distribution, cumulative probabilities of the WSD
222 series were obtained and transformed to standardized units (SAPEI) using the classical
223 approach of Barton et al. (1965).

224 **2.2.2 Construction of SCDHI**

225 The SCDHI was established through copula theory (a brief introduction on copula
226 theory is shown in supplementary materials), which can combine the candidate
227 variables into one numerical expression. This approach not only realizes a projection
228 from multiple dimensions to a single dimension, but also the marginal distributions of
229 the candidate variables combined with their original structures can be fully preserved
230 within the constructed joint distribution. Hence, the copula-based index provides an
231 objective description of the compound events (Hao et al., 2018b; Terzi et al., 2019).

232 There are many copula families available, which have widely been used for jointing
233 bivariate distributions (Terzi et al., 2019). Among them, Clayton, Gumbel, Normal, T,
234 and Frank copula perform well for jointing bivariate hydrometeorological variables
235 (Ayantobo et al., 2018; Liu et al., 2019), and thus were employed to establish the
236 bivariate joint probability distribution in this study. Assuming, the two random
237 Gaussian variables X and Y representing SAPEI and STI, respectively, the compound
238 dry-hot event can be identified as one variable X lower than or equal to a threshold x ,
239 and the other variable Y higher than a threshold y at the same time. The joint

240 probability P of the compound dry-hot event can then be expressed as:

$$p = P(X \leq x, Y \geq y) = u - c(u, v) \quad (2)$$

241 where u was the X marginal distribution, and $c(u, v)$ was the joint probability
242 distribution.

243 This joint cumulative probability P could be treated as an indicator, where smaller
244 P values denote more severe condition of compound dry-hot event. However, P to
245 the given marginal sets, P values in different seasons or areas reflected different
246 conditions and are thus not comparable. Hence, the joint probability P was
247 transformed to a uniform distribution by fitting a distribution F , which was then
248 standardized as an indicator to characterize compound dry-hot events. Once the P
249 series at each day were fitted to a copula, the P series were transformed to standardized
250 units. SCDHI can be estimated by taking the inverse of joint cumulative probability (p)
251 as:

$$SCDHI = \varphi^{-1}(F(P(X \leq x, Y \geq y))) \quad (3)$$

252 where φ is the standard normal distribution function. the distribution F was
253 estimated based on the Yeo-Johnson transformation formula (Yeo and Johnson, 2000).

254 Following the categories of compound dry and hot conditions as suggested by (Wu
255 et al., 2020), we defined five categories of compound dry and hot conditions, including
256 abnormal, light, moderate, heavy and extreme compound drought-hot, as shown in
257 Table 1.

258 We used Akaike information criterion, Bayesian information Criterion, and
259 Kolmogorov-Smirnov statistics as goodness-of-fit measures to select an appropriate
260 copula. These statistical measures have been commonly used for estimating the
261 goodness of fit of a proposed cumulative distribution function to a given empirical
262 distribution function (Liu et al., 2019; Terzi et al., 2019). The statistics of the three
263 metrics are presented in Fig. S1-3. According to the evaluation metrics, the Frank
264 copula was utilized to establish the joint probability function and construct SCDHI in
265 this study. Note that the SCDHI under three future scenarios is also used the Frank
266 copula, while the parameters are assessed by future scenarios data. The SCDHI
267 development was illustrated in Fig. S4.

268 Furthermore, to verify the ability of SCDHI to capture the compound dry and hot
269 event, three verification metrics were used (i.e., probability of detection, false alarm
270 ratio, and critical success index) (Winston and Ruthi, 1986).

$$\textit{Probability of detection} = \textit{hit}/(\textit{hit} + \textit{miss}) \quad (4)$$

$$\textit{False alarm ratio} = \textit{false alarm} / (\textit{hit} + \textit{false alarm}) \quad (5)$$

$$\textit{Critical success index} = \textit{hit} / (\textit{hit} + \textit{false alarm} + \textit{miss}) \quad (6)$$

271 where *hit* (observed drought-hot) refers to the number of grids when SAPEI and
272 STI is subjected to grade 1-4 and SCDHI is subjected to grade 1-4; *Miss* denotes the
273 number of grids when SAPEI and STI is between grade 1-4 and SCDHI is subjected to
274 other grades than grade 1-4; *False alarm* denotes the number of grids when SAPEI and
275 STI is subjected to other grades than grade 1-4 but SCDHI is subjected to grades of
276 grade 1-4.

277 **3 Results and Discussion**

278 **3.1 Evaluation of SAPEI**

279 The SCDHI was established based on the STI and daily-scale drought index, i.e.,
280 SAPEI. However, no previous studies have tested the (daily) drought monitoring
281 performance of SAPEI. When developing a drought index, rigorous testing is required
282 with respect to its applicability before it is applied in drought monitoring. Fig. 2 shows
283 the spatial distributions and density of the correlations between SAPEI and
284 SPEI/PDSI/soil moisture across China. The monthly mean SAPEI at 3-, 6-, 9- and 12-
285 month scale all showed strong agreement with the SPEI in China, with correlation
286 coefficients higher than 0.8 ($p < 0.01$), indicating that the monthly SAPEI at multiple
287 time scale calculated from the daily value could have the same capability of monthly
288 drought monitoring as SPEI. The 3-, 6-, 9- and 12-month SAPEI generally showed good
289 correlation with PDSI, and 3-month SAPEI and PDSI generally correlate closely, with
290 correlation coefficients higher than 0.6 ($p < 0.01$). For daily SAPEI at 12-month scale
291 and soil moisture, a close correlation was detected in south and north China, while
292 relatively weak correlation is found in Midwest China. The correlation between SAPEI
293 and soil moisture increased in magnitude at time scales of 3-9 months. For 12-month
294 SAPEI, mean correlation coefficient reached about 0.5 for whole China. This
295 phenomenon implied that the short-time scale SAPEI was more sensitive to
296 precipitation change, and thus could be more suitable for meteorological drought, while
297 the long-time scale (more than five month) SAPEI was more closely related to soil
298 moisture and can be applied for agricultural drought monitoring. Overall, these analyses
299 indicate that the SAPEI at daily and monthly scale showed reliability in drought
300 monitoring.

301 To further test the drought monitoring performance of the SAPEI, typical drought

302 events were chosen as case studies. During recent decades, several well-known large-
303 scale drought events have hit China, including the droughts in winter of 2009 to spring
304 of 2010, and in 2011 (Lu et al., 2014; Yu et al., 2019). In this study, the drought regimes
305 during these events were taken as case studies to evaluate the drought monitoring
306 performance of SAPEI at 3-month time scales (Sun and Yang, 2012). We firstly showed
307 the monthly evolution of these events by the monthly mean SAPEI, SPEI, and PDSI,
308 and then analyzed the daily evolution of drought in space and time in the most affected
309 areas according to SAPEI and soil moisture.

310 **3.2.1 Drought events during 2009-2010**

311 As shown in Fig. S5, the monthly evolution in 2009/10 drought based on SAPEI
312 was generally similar with that of SPEI and PDSI. This drought started to appear in
313 most of China (except for the central and northeast China) in September 2009, and then
314 persisted in most of China during October to December 2009. During January and April
315 in 2010, severe drought persisted in southwest China, while drought in the rest of China
316 gradually disappeared in this period. After that, dry conditions in southwest China
317 gradually relieved from May to June in 2010, but did not disappear.

318 Despite being located in the humid climate zone, southwest China suffered from
319 exceptional drought during the autumn of 2009 to the spring of 2010 (Lin et al., 2015).
320 During this drought, more than 16 million people and 11 million livestock faced
321 drinking water shortages, with direct economic losses estimated at 19 billion yuan in
322 southwest China (Lin et al., 2015). We selected this event in southwest China as the
323 first case study, and reveal detailed spatial and temporal change of this event at daily
324 scale based on SAPEI and soil moisture (Fig. 3 and 4). During September 1 to 30 of
325 2009, the drought started to appear in the region, and dry conditions became worse and
326 spread throughout nearly the entire southwest China from October 1 to November 15

327 of 2009. Severe dry conditions then stayed in the region for 152 days from November
328 15 to April 15 of 2010, with high intensity. Afterwards, severe drought was gradually
329 relieved from April 15 to June 15. The drought diminished over time in most parts of
330 southwest China by the end of June.

331 **3.2.2 Drought events in 2011**

332 As shown in Fig. S6. The 2011 drought monthly pattern monitored by SAPEI are
333 generally consistent with those by SPEI and PDSI. The drought mainly started in north
334 China in January, while in March it spread to most of China, and severe dry conditions
335 persisted in most areas during April to May. In August, the drought mainly moved to
336 southward. Severe drought persisted in southwest China during September and October,
337 but it then gradually faded away. The results monitored by the SAPEI are generally
338 consisted with the findings of Lu et al. (2014).

339 The 2011 drought event was particularly unusual in the middle and lower reaches
340 of the Yangtze River Basin (MLR-YRB). The MLR-YRB is generally in a wet
341 condition, nevertheless, suffered its worst drought in the 50 years during the spring.
342 The severe drought caused shortage of drinking water for 4.2 million people. 3.7 million
343 hectares of crops were damaged or destroyed. Moreover, the heavy drought led to more
344 than 1,300 lakes devoid of all water in Hubei province (Xu et al., 2015). The temporal
345 and spatial evolution of this event in MLR-YRB described by daily SAPEI and soil
346 moisture was shown in Fig. 5-6. The drought started to appear in the north part of the
347 MLR-YRB in early February of 2011, and then gradually expanded to the whole MLR-
348 YRB during early February and March 15. The severe drought condition persisted in
349 this region for 78 days (from March 15 to May 31). Afterwards, there was a tendency
350 toward alleviating drought conditions, and most of MLR-YRB was under light and
351 moderate drought conditions.

352 The previous detailed analysis showed that the SAPEI not only captures monthly
353 characteristics of droughts, but also has the potential to track droughts at sub-monthly
354 scale (Li et al., 2020b). Though the input data (including precipitation and potential
355 evapotranspiration) of SAPEI are similar to SPEI, the rationale of the index is different
356 from SPEI. It was calculated for each day and considers the water surplus or deficit of
357 that day and the previous days. SPEI was commonly employed to monitor and analyze
358 the monthly or longer-scale droughts (Vicente-Serrano et al., 2010). It thus may not be
359 appropriate to apply the SPEI at shorter timescales (e.g., daily or weekly), because of
360 the inherent problem in the construction of the index. Although SPEI gives a full and
361 equal consideration to the water surplus or deficit in the period of the considered time
362 scale, it does not consider the water surplus or deficit in the days before the period. If
363 the scale is very short, this may cause problems. For a 7-day period, for example, if
364 there is no precipitation during the period, it may be regarded as a drought period when
365 compared with historical records (the method used by the SPEI); however, if there is a
366 heavy precipitation just before the period, then the 7-day period probably remains wet
367 and is unlikely to experience drought condition during such a short time. Previous
368 studies have demonstrated the disadvantage of SPEI for short-time scale drought
369 monitoring (Lu, 2009; Lu et al., 2014; Li et al., 2020b).

370 Soil moisture would be the most appropriate variable for agriculture drought
371 monitoring and analyses (Mishra and Singh, 2010). However, there are few long-term
372 and large-scale observational soil moisture datasets due to insufficient observation
373 stations around the world, especially for developing regions, which limits its wide use
374 in drought monitoring and analyses (Seneviratne et al., 2010). Thus, using
375 observational hydrometeorological datasets, the complex physical process models, such
376 as the variable infiltration capacity model, are widely used to simulate the soil moisture

377 (Liang et al., 1996; Xia et al., 2018). However, running such models requires highly
378 trained personnel not usually available at local agencies. In addition, when the model
379 is used locally, it generally needs to be calibrated and verified by observational datasets
380 (Xia et al., 2018; Zhou et al., 2019). This certainly limits the wide use of soil moisture
381 as a drought indicator.

382 In summary, the SAPEI meets the requirements of a drought index, given the fact
383 that it shows reliable and robust ability for drought analysis and monitoring. Like the
384 SPEI, SAPEI includes multiple time scales (3-, 6-, 9-, and 12- month) to monitor
385 droughts at monthly resolution and is relatively sensitive to soil moisture variation.
386 However, SAPEI has the advantage over SPEI regarding sub-monthly drought
387 monitoring. Such an index could help fill a gap between science and applications in that
388 it would be operationally tractable for detecting and monitoring both short-term and
389 sustained droughts.

390 **3.2 Evaluation of SCDHI**

391 The SCDHI was developed by joining the marginal distribution of the SAPEI and
392 STI. Though the copula method has been widely utilized to connect bivariate
393 distribution, the property of SCDHI in capturing compound dry-hot events still needs
394 to be tested. Fig. 7 shows the spatial pattern and density for probability of detection,
395 false alarm ratio, and critical success index when the drought and hot events observed
396 by SAPEI and STI, respectively, were related to compound drought-hot event detected
397 by SCDHI at 3-, 6-, 9- and 12-monthly scale. As shown in Fig. 7, probability of
398 detection is close to 1 and false alarm ratio is close to 0, implying that SCDHI can well
399 detect in most of the areas where the droughts and hots were detected by SAPEI and
400 STI. The values of critical success index indicated that the ratios of drought-hot affected
401 areas detected by SAPEI and STI to the drought and hot areas detected by SCDHI were

402 close to one. Overall, these analyses implied that SCDHI can well monitor droughts
403 and hots that can be successfully captured by SAPEI and STI. The SCDHI thus detects
404 compound dry-hot events that are identified separately by the coincidence of low
405 SAPEI and high STI. In addition, the SCDHI detects events that are very extreme in
406 either the SAPEI or the STI and moderate in the other variable but thus still cause
407 substantial damage (Zscheischler et al., 2017b). Furthermore, the SCDHI is able to
408 quantify the magnitude of compound dry-hot events.

409 To further test the drought-heat monitoring performance of the SCDHI, two typical
410 compound dry-hot events were chosen as case studies according to the Yearbook of
411 Meteorological Disasters in China. One was a well-known compound drought and
412 heatwave striking Sichuan-Chongqing region with serious consequences during
413 summer of 2006 (Wu et al., 2020), and the other occurred in southern China with
414 adverse impacts on agriculture during July to September of 2009 (Wang et al., 2010).
415 Sichuan-Chongqing region experienced continuous extreme temperature during mid-
416 June to late August 2006. The duration and severity of this hot event were the worst on
417 the historical record. Simultaneously, a heavy drought occurring once in 100 years hit
418 this region. During this compound event, a population of over ten million was
419 confronted with drinking water shortage, about twenty thousand km² of cropland
420 suffered serious losses, and more than one hundred times forest fire broke out. Local
421 governments issued the most serious arid warning (Zhang et al., 2008). Thus, we take
422 this typical drought-hot event as first case studies to evaluate the drought/hot
423 monitoring performance of SCDHI. The monthly spatial pattern of this compound event
424 in Sichuan-Chongqing region is shown in Fig. S7, indicating that Sichuan-Chongqing
425 region during summer in 2006 experienced the moderate to extreme compound dry and
426 hot conditions. Fig. 8 maps the spatial pattern of this compound event and its impact on

427 vegetation from mid-June to late August. This event started to appear in Sichuan-
428 Chongqing region in mid-June 2006, and gradually spread throughout the whole
429 Sichuan-Chongqing region during June 19 to 26. The moderate dry-hot condition then
430 persisted in the entire Sichuan-Chongqing region from June 27 to August 5 in 2006,
431 lasting for 40 days. The negative leaf area index was scattered in some of the dry-hot
432 affected areas. However, during August 6 to 21, the drought-hot event became even
433 more severe with the onset of extremely hot temperatures, causing negative vegetation
434 anomalies in most of the affected areas.

435 The monthly spatial pattern of another compound event in southern China during
436 July to September of 2009 is shown in Fig. S8. Overall moderate to heavy compound
437 dry and hot conditions are observed at monthly scale in this region. However, this event
438 showed large fluctuation at weekly scale. According to the Yearbook, the hot event was
439 divided into two periods: the first stage was from early to late July, and the other stage
440 was from mid-August to early September. The fluctuating compound event caused
441 adverse impact of crop pollination and grain filling, resulting in decrease of crop
442 production. Fig. 9 maps the spatial pattern of this event and its impact on leaf area index.
443 In the first stage, the drought-hot event hit the most of southern China during July 5 to
444 12, and then it became severe in the west part of southern China during July 13 to 20.
445 However, the hot event suddenly disappeared from July 21 to 28, leading to
446 disappearance of the compound event in most of southern China (Fig. 9a). Afterward,
447 the compound event hit this region again from August 6 to 13, and its intensity was
448 strong during August 14 to 21, with severe hot conditions. Subsequently, the intensity
449 and spatial extent of the compound event faded away in north of southern China during
450 August 22 to 29. This event extended to most of this region again from August 30 to
451 September 14, with severe dry and hot condition. The compound events still stayed in

452 this region from September 15 to 22 (Fig. 9b). Despite the short-term event, the abnormal
453 change in vegetation was found in most of the dry-hot affected areas. This complex
454 event indicates that monthly analyses of the event can provide an overall situation, but
455 is not be able to capture the serious dry and hot conditions caused by a short-term
456 extreme climate anomaly at shorter time scales. Though such short-term compound
457 event only lasted for days or weeks, they lead to large agricultural losses if they occur
458 within sensitive stages in crop development (i.e., pollination and grain filling)
459 (Mazdiyasni and AghaKouchak, 2015). To provide timely information of the
460 compound dry-hot events, short-time scale analyses and monitoring of such events are
461 essential.

462 Overall, the changes in these two compound dry-hot events based on SCDHI are
463 consistent with the national weather records (<http://www.weather.com.cn/zt/kpzt/>) and
464 the Yearbook of Meteorological Disasters in China 2010. In summary, the SCDHI is
465 able to robustly and reliably capture compound dry-hot events at sub-monthly scale,
466 and potentially provide a new tool to objectively and quantitatively analyze and monitor
467 the characteristics of compound dry-hot events in time and space.

468 **3.3 Application**

469 Here, we evaluate and compare the spatiotemporal variation of characteristics of
470 compound dry-hot events in China during growing season (April-September), because
471 such events can more easily cause adverse impact on agriculture and ecosystem during
472 these periods (Hao et al., 2018; Wu et al., 2019). More precisely, the compound dry-
473 hot events from 1961 to 2018 were identified based on 3-month scale SCDHI and run
474 theory (Wu et al., 2018), after which the frequency, duration, severity, and intensity of
475 these events were analyzed (A specific case to identify compound dry-hot event is
476 shown in Fig. S9). We then projected their future characteristics changes under the RCP

477 2.6, 4.5 and 8.5 from 2050 to 2100. Given that short-term concurrent dry and hot events
478 generally persist for at least weeks (Otkin et al., 2018), only the events lasting for more
479 than two weeks were considered in this study.

480 Fig. 10 shows spatial patterns of characteristics of the compound dry-hot events. A
481 high frequency of compound events was detected in southern China, with occurrence
482 of every two years on average, in contrast, the eastern Tibet Plateau and northeast China
483 experienced fewer compound events (Fig. 10a), which was generally consistent with
484 the previous studies (Liu et al., 2020; Wang et al., 2016). The compound dry-hot event
485 generally lasted for about twenty-five to thirty-five days in most of China, while in east
486 Tibet Plateau, the compound dry-hot event persisted for less than twenty days (Fig.
487 10b). The severity and intensity of the compound dry-hot event presented relatively
488 similar patterns and showed that most of eastern China experienced high severity and
489 intensity (Fig. 10c-d). Overall, southern China suffered more frequent compound dry-
490 hot events, with higher severity and intensity. Southern China is a humid region where
491 evapotranspiration is mainly controlled by energy supply because soil moisture is
492 usually sufficient. For given adequate soil moisture in the initiation of drought,
493 evaporative demand can increase rapidly during a short period when strong, transient
494 meteorological changes (such as extreme temperature) occur, which in turn exhaust soil
495 moisture to intensify drought conditions (Zhang et al., 2019, Otkin et al., 2018).
496 Moreover, vegetation over south China is usually abundant and plants tend to suck more
497 water from the soil when high temperatures occur, causing evapotranspiration increase
498 and soil moisture decline (Li et al., 2020c; Wang et al., 2016). More surface sensible
499 heat fluxes are thus transferred to the near-surface atmosphere to further increase air
500 temperatures (Mo and Lettenmaier, 2015). These land-atmosphere interactions
501 altogether cause the Bowen ratio to increase (Otkin et al., 2013, 2018), creating a

502 favorable condition for short-term concurrence droughts and hots. Therefore,
503 compound dry-hot event is more likely to occur in humid regions with higher severity
504 and intensity.

505 Fig. 11 illustrates the spatial patterns of change in frequency, duration, severity, and
506 intensity of the compound dry-hot events under RCP 2.6, 4.5, and 8.5 scenarios.
507 According to Fig. 11a, the future (2050-2100) compound dry-hot event frequency under
508 three scenarios in most of east China will increase by about one to three times with
509 respect to the reference period (1961-2018). Under RCP 8.5 scenario, compound dry-
510 hot event at about 4% of the study region is expected to markedly increase by more
511 than five times, which are scattered in the central to west parts of China. The duration
512 of compound dry-hot event across the east of the study region will mainly show an
513 increase of about 0.5 times, while duration in mid-west China potentially increases by
514 approximately 1.5 times under RCP 8.5 scenarios (Fig. 11b). The spatial pattern of
515 future severity change is similar to the duration; severity in most of east China is
516 projected to increase by about 0.5 time under three scenarios; however, compound dry-
517 hot event severity over mid-west China is expected to more than triple under RCP 8.5
518 (Fig. 11c). The compound dry-hot event intensity in most of the study region exhibits
519 slight increase for all scenarios in comparison to the historical period.

520 Global warming is very likely to exacerbate the prevalence of the compound dry-
521 hot events (Pfleiderer et al., 2019). The cumulative density functions of the future
522 variations in compound dry-hot event characteristics considering only temperature and
523 all variable changes were quantified, and the result is shown in Fig. 12. The frequency
524 and intensity of the future variations in compound dry-hot event do not show large
525 difference between two scenarios, while duration and severity display great increase
526 due to temperature variation, as marked by the movement towards the right side of the

527 cumulative density curves. Increasing temperature could lead to remarkable increase
528 evapotranspiration, and thus causing more surface sensible heat fluxes into atmosphere
529 (Mo and Lettenmaier, 2015; Zhang et al., 2019). These land-atmosphere interactions
530 altogether cause the Bowen ratio to increase (Otkin et al., 2013, 2018), creating a
531 favorable condition for concurrence dries and hots. In short, temperature could be
532 generally the primary factor increasing the compound dry-hot severity and duration
533 (Cook et al., 2014). In addition, trends are often present in individual variables, while
534 can also occur in the dependence between drivers of compound events, which
535 consequently affects associated risks. The (negative) correlation between seasonal
536 mean summer temperature and precipitation is projected to intensify in many land
537 regions, leading to more frequent extremely dry and hot conditions (Kirono et al., 2017;
538 Zscheischler and Seneviratne, 2017a), while variation in compound dry-hot event due
539 to the complex interaction between climate variables is need further studied
540 (Zscheischler et al., 2020). Overall, the frequency, severity, duration, and intensity of
541 the compound dry-hot events in China under global warming will increase significantly.
542 Effective measures need to be implemented to decrease the CO₂emissions for
543 compound dry and hot event mitigation.

544 **4 Conclusions**

545 Under global warming, the compound dry and hot event tends to more frequent and
546 short-lived (i.e., days or weeks). Correspondingly, a compound drought and heat index
547 should be able to monitor such event at sub-monthly scales in order to timely reflect
548 dry and hot condition evolution. In this study, we developed a multiple time scale (e.g.,
549 3-, 6-, 9, and 12- month) compound drought and heat index, termed as SCDHI, to
550 monitor short-time (e.g., days or weeks) and long-time (e.g., months) compound event.
551 This index was established based on the daily drought index (i.e., SAPEI) and

552 Standardized Temperature Index (STI) using a joint probability distribution method.
553 Using the SCDHI, we then quantitatively investigated the characteristics (i.e., frequency,
554 intensity, severity, and duration) of the compound dry-hot events in China in historical
555 period (1961-2018), and revealed how they would change in the future (2050-2100)
556 under representative concentration pathway (RCP) 2.6, 4.5, and 8.5 scenarios. The main
557 conclusions of this study are presented as follows: The SCDHI can well monitor
558 simultaneous dries and hots detected by SAPEI and STI. The monthly SCDHI can
559 provide an overall situation of the compound dry and hot conditions, but sub-monthly
560 SCDHI can well capture fluctuation of simultaneous dries and hots within a month. It
561 also can reflect the impact of the compound dry and hot event on vegetation anomalies.
562 The SCDHI can offer a new tool to quantitatively measure the characteristics of the
563 compound dry-hot events. It also can provide detailed information such as the initiation,
564 development, decay, and tendency of the compound event for decision-makers and
565 stakeholders to make early and timely warning. In the case study of the China, the
566 southern China suffered more frequent the compound dry-hot event, with higher
567 severity and intensity. The compound dry-hot event mainly lasted for twenty-five to
568 thirty-five days in China. The frequency, duration, severity, and intensity of compound
569 events will intensify throughout the China in future. The frequency will increase by
570 about one to three times with respect to the reference period. A region with fewer
571 compound event (< 5) would exhibit a multi-fold (more than five times) increase in the
572 future. The duration across east areas mainly increased by 0.5 times, while severity
573 project to increase by about 0.5 to 1 times.

574

575

576

577

578 **Data availability.** The observed meteorological datasets are available at
579 <http://cdc.nmic.cn/home.do>. The CMIP5 datasets are available at <https://esgf.llnl.gov>.

580

581 **Author Contributions.** Conceived and designed the experiments: JL, SW. Performed
582 the experiments: JL, SW. Analyzed the data: JL. Wrote and edited the paper: JL, SW,
583 ZW, JZ, SG, XC.

584

585 **Competing interests.** The authors declare that they have no conflict of interest.

586

587 **Acknowledgement**

588 The research is financially supported by the National Natural Science Foundation
589 of China (51879107, 51709117), the Guangdong Basic and Applied Basic Research
590 Foundation (2019A1515111144), and the Water Resource Science and Technology
591 Innovation Program of Guangdong Province (2020-29).

592

593 **References**

594 Allen, R. G., Pereira, L. S., Raes, D. and Smith, M.: Crop evapotranspiration:
595 Guidelines for computing crop requirements, Irrig. Drain. Pap. No. 56, FAO,
596 doi:10.1016/j.eja.2010.12.001, 1998.

597 Ayantobo, O. O., Li, Y., Song, S., Javed, T. and Yao, N.: Probabilistic modelling of
598 drought events in China via 2-dimensional joint copula, *J. Hydrol.*, 559, 373–391,
599 doi:10.1016/j.jhydrol.2018.02.022, 2018.

600 Barton, D. E., Abramovitz, M. and Stegun, I. A.: Handbook of Mathematical Functions
601 with Formulas, Graphs and Mathematical Tables., *J. R. Stat. Soc. Ser. A*,

602 doi:10.2307/2343473, 1965.

603 Bi, H., Ma, J., Zheng, W. and Zeng, J.: Comparison of soil moisture in GLDAS model
604 simulations and in situ observations over the Tibetan Plateau, *J. Geophys. Res.*,
605 doi:10.1002/2015JD024131, 2016.

606 Chen, L., Chen, X., Cheng, L., Zhou, P. and Liu, Z.: Compound hot droughts over
607 China: Identification, risk patterns and variations, *Atmos. Res.*, 227(May), 210–
608 219, doi:10.1016/j.atmosres.2019.05.009, 2019.

609 Cook, B. I., Smerdon, J. E., Seager, R., and Coats, S.: Global warming and 21 st century
610 drying. *Climate Dynamics*, 43(9-10), 2607-2627, 2014.

611 Feng, X., Fu, B., Piao, S., Wang, S., Ciais, P., Zeng, Z., Lü, Y., Zeng, Y., Li, Y., Jiang,
612 X. and Wu, B.: Revegetation in China’s Loess Plateau is approaching sustainable
613 water resource limits, *Nat. Clim. Chang.*, doi:10.1038/nclimate3092, 2016.

614 Ford, T. W., McRoberts, D. B., Quiring, S. M. and Hall, R. E.: On the utility of in situ
615 soil moisture observations for flash drought early warning in Oklahoma, USA,
616 *Geophys. Res. Lett.*, doi:10.1002/2015GL066600, 2015.

617 Hao, Z., Hao, F., Singh, V. P., Xia, Y., Shi, C. and Zhang, X.: A multivariate approach
618 for statistical assessments of compound extremes, *J. Hydrol.*, 565, 87–94,
619 doi:10.1016/j.jhydrol.2018.08.025, 2018a.

620 Hao, Z., Hao, F., Singh, V. P. and Zhang, X.: Quantifying the relationship between
621 compound dry and hot events and El Niño–southern Oscillation (ENSO) at the
622 global scale, *J. Hydrol.*, 567, 332–338, doi:10.1016/j.jhydrol.2018.10.022, 2018b.

623 Hao, Z., Hao, F., Singh, V. P. and Zhang, X.: Statistical prediction of the severity of
624 compound dry-hot events based on El Niño-Southern Oscillation, *J. Hydrol.*, 572,
625 243–250, doi:10.1016/j.jhydrol.2019.03.001, 2019.

626 Hunt, E. D., Hubbard, K. G., Wilhite, D. A., Arkebauer, T. J. and Dutcher, A. L.: The

627 development and evaluation of a soil moisture index. *Int. J. Climatol.*, 29(5), 747-
628 759, doi.org/10.1002/joc.1749, 2009.

629 James, S., Complex, B., Black, S. J., Health, O. and Ando, H.: The synergy between
630 drought and extremely hot summers in the Mediterranean, *Biochem. J.*, 2010.

631 Jiang, D., Tian, Z. and Lang, X.: Reliability of climate models for China through the
632 IPCC Third to Fifth Assessment Reports, *Int. J. Climatol.*, doi:10.1002/joc.4406,
633 2016.

634 Kirono, D. G. C., Hennessy, K. J. and Grose, M. R.: Increasing risk of months with low
635 rainfall and high temperature in southeast Australia for the past 150 years, *Clim.*
636 *Risk Manag.*, doi:10.1016/j.crm.2017.04.001, 2017.

637 Koster, R. D., Schubert, S. D., Wang, H., Mahanama, S. P. and Deangelis, A. M.: Flash
638 drought as captured by reanalysis data: Disentangling the contributions of
639 precipitation deficit and excess evapotranspiration, *J. Hydrometeorol.*,
640 doi:10.1175/JHM-D-18-0242.1, 2019.

641 Liang, X., Wood, E. F., and Lettenmaier, D. P.: Surface soil moisture parameterization
642 of the VIC-2L model: Evaluation and modification. *Global and Planetary Change*,
643 13(1-4), 195-206, 1996.

644 Li, J., Wang, Z., Wu, X., Chen, J., Guo, S., and Zhang, Z.: A new framework for
645 tracking flash drought events in space and time. *Catena*, 194, 104763, 2020a.

646 Li, J., Wang, Z., Wu, X., Xu, C.-Y., Guo, S. and Chen, X.: Toward Monitoring Short-
647 Term Droughts Using a Novel Daily-Scale, Standardized Antecedent Precipitation
648 Evapotranspiration Index, *J. Hydrometeorol.*, 891–908, doi:10.1175/jhm-d-19-
649 0298.1, 2020b.

650 Li, J., Wang, Z., Wu, X., Guo, S., and Chen, X.: Flash droughts in the Pearl River Basin,
651 China: Observed characteristics and future changes. *Sci. Total Environ.*, 707,

652 136074, 2020c.

653 Lin, W., Wen, C., Wen, Z. and Gang, H.: Drought in Southwest China: A Review,
654 Atmos. Ocean. Sci. Lett., 8(6), 339–344, doi:10.3878/AOSL20150043, 2015.

655 Liu, Z., Wang, Y., Shao, M., Jia, X., Li, X: Spatiotemporal analysis of multiscalar
656 drought characteristics across the Loess Plateau of China. J. Hydrol., 534, 281-
657 299, doi.org/10.1016/j.jhydrol.2016.01.003, 2016,

658 Liu, Y., Zhu, Y., Ren, L., Singh, V. P., Yang, X. and Yuan, F.: A multiscalar Palmer
659 drought severity index, Geophys. Res. Lett., 44(13), 6850–6858,
660 doi:10.1002/2017GL073871, 2017.

661 Liu, Y., Zhu, Y., Ren, L., Yong, B., Singh, V. P., Yuan, F., Jiang, S. and Yang, X.: On
662 the mechanisms of two composite methods for construction of multivariate
663 drought indices, Sci. Total Environ., 647, 981–991,
664 doi:10.1016/j.scitotenv.2018.07.273, 2019.

665 Liu, Y., Zhu, Y., Zhang, L., Ren, L., Yuan, F., Yang, X. and Jiang, S.: Flash droughts
666 characterization over China: From a perspective of the rapid intensification rate,
667 Sci. Total Environ., doi:10.1016/j.scitotenv.2019.135373, 2020.

668 Lu, E.: Determining the start, duration, and strength of flood and drought with daily
669 precipitation: Rationale, Geophys. Res. Lett., 36(12), 1–5,
670 doi:10.1029/2009GL038817, 2009.

671 Lu, E., Cai, W., Jiang, Z., Zhang, Q., Zhang, C., Higgins, R. W. and Halpert, M. S.:
672 The day-to-day monitoring of the 2011 severe drought in China, Clim. Dyn., 43(1–
673 2), 1–9, doi:10.1007/s00382-013-1987-2, 2014.

674 Mo, K. C. and Lettenmaier, D. P.: Heat wave flash droughts in decline, Geophys. Res.
675 Lett., doi:10.1002/2015GL064018, 2015.

676 Mo, K. C. and Lettenmaier, D. P.: Precipitation deficit flash droughts over the United

677 States, *J. Hydrometeorol.*, doi:10.1175/JHM-D-15-0158.1, 2016.

678 Mazdiyasi, O. and AghaKouchak, A.: Substantial increase in concurrent droughts and
679 heatwaves in the United States, *Proc. Natl. Acad. Sci. U. S. A.*, 112(37), 11484–
680 11489, doi:10.1073/pnas.1422945112, 2015.

681 Manning, C., Widmann, M., Bevacqua, E., Van Loon, A. F., Maraun, D. and Vrac, M.:
682 Increased probability of compound long-duration dry and hot events in Europe
683 during summer (1950-2013). *Environmental Research Letters*, 14(9), 094006,
684 2019.

685 Osman, M., Zaitchik, B. F., Badr, H. S., Christian, J. I., Tadesse, T., Otkin, J. A. and
686 Anderson, M. C.: Flash drought onset over the Contiguous United States:
687 Sensitivity of inventories and trends to quantitative definitions, *Hydrol. Earth Syst.*
688 *Sci. Discuss.*, doi.org/10.5194/hess-2020-385, in review, 2020.

689 Otkin, J. A., Anderson, M. C., Hain, C., Mladenova, I. E., Basara, J. B. and Svoboda,
690 M.: Examining rapid onset drought development using the thermal infrared-based
691 evaporative stress index, *J. Hydrometeorol.*, doi:10.1175/JHM-D-12-0144.1, 2013.

692 Otkin, J. A., Svoboda, M., Hunt, E. D., Ford, T. W., Anderson, M. C., Hain, C. and
693 Basara, J. B.: Flash droughts: A review and assessment of the challenges imposed
694 by rapid-onset droughts in the United States, *Bull. Am. Meteorol. Soc.*, 99(5),
695 911–919, doi:10.1175/BAMS-D-17-0149.1, 2018.

696 Pflleiderer, P., Schleussner, C. F., Kornhuber, K. and Coumou, D.: Summer weather
697 becomes more persistent in a 2 °C world, *Nat. Clim. Chang.*, 9(9), 666–671,
698 doi:10.1038/s41558-019-0555-0, 2019.

699 Rodell, M., Houser, P. R., Jambor, U., Gottschalck, J., Mitchell, K., Meng, C. J.,
700 Arsenault, K., Cosgrove, B., Radakovich, J., Bosilovich, M., Entin, J. K., Walker,
701 J. P., Lohmann, D. and Toll, D.: The Global Land Data Assimilation System, *Bull.*

702 Am. Meteorol. Soc., doi:10.1175/BAMS-85-3-381, 2004.

703 Röhlisberger, M. and Martius, O.: Quantifying the Local Effect of Northern
704 Hemisphere Atmospheric Blocks on the Persistence of Summer Hot and Dry
705 Spells, *Geophys. Res. Lett.*, doi:10.1029/2019GL083745, 2019.

706 Schumacher, D. L., Keune, J., van Heerwaarden, C. C., Vilà-Guerau de Arellano, J.,
707 Teuling, A. J. and Miralles, D. G.: Amplification of mega-heatwaves through heat
708 torrents fuelled by upwind drought, *Nat. Geosci.*, 12(9), 712–717,
709 doi:10.1038/s41561-019-0431-6, 2019.

710 Sedlmeier, K., Feldmann, H. and Schädler, G.: Compound summer temperature and
711 precipitation extremes over central Europe, *Theor. Appl. Climatol.*,
712 doi:10.1007/s00704-017-2061-5, 2018.

713 Stagge, J. H., Tallaksen, L. M., Gudmundsson, L., Van Loon, A. F. and Stahl, K.:
714 Candidate Distributions for Climatological Drought Indices (SPI and SPEI), *Int. J.*
715 *Climatol.*, doi:10.1002/joc.4267, 2015.

716 Seneviratne, S. I., Corti, T., Davin, E. L., Hirschi, M., Jaeger, E. B., Lehner, I., .and
717 Teuling, A. J.: Investigating soil moisture–climate interactions in a changing
718 climate: A review. *Earth-Science Reviews*, 99(3-4), 125-161, 2010.

719 Sun, C. and Yang, S.: Persistent severe drought in southern China during winter-spring
720 2011: Large-scale circulation patterns and possible impacting factors, *J. Geophys.*
721 *Res. Atmos.*, doi:10.1029/2012JD017500, 2012.

722 Sun, C. X., Huang, G. H., Fan, Y., Zhou, X., Lu, C. and Wang, X. Q.: Drought
723 Occurring With Hot Extremes: Changes Under Future Climate Change on Loess
724 Plateau, China, *Earth’s Futur.*, 7(6), 587–604, doi:10.1029/2018EF001103, 2019.

725 Swain, D. L., Langenbrunner, B., Neelin, J. D. and Hall, A.: Increasing precipitation
726 volatility in twenty-first-century California, *Nat. Clim. Chang.*, 8(5), 427–433,

727 doi:10.1038/s41558-018-0140-y, 2018.

728 Taylor, K. E., Stouffer, R. J. and Meehl, G. A.: An overview of CMIP5 and the
729 experiment design, *Bull. Am. Meteorol. Soc.*, doi:10.1175/BAMS-D-11-00094.1,
730 2012.

731 Terzi, S., Torresan, S., Schneiderbauer, S., Critto, A., Zebisch, M. and Marcomini, A.:
732 Multi-risk assessment in mountain regions: A review of modelling approaches for
733 climate change adaptation, *J. Environ. Manage.*, 232(September 2018), 759–771,
734 doi:10.1016/j.jenvman.2018.11.100, 2019.

735 Vicente-Serrano, S. M., Beguería, S. and López-Moreno, J. I.: A multiscalar drought
736 index sensitive to global warming: The standardized precipitation
737 evapotranspiration index, *J. Clim.*, 23(7), 1696–1718,
738 doi:10.1175/2009JCLI2909.1, 2010.

739 Wang, L., Yuan, X., Xie, Z., Wu, P. and Li, Y.: Increasing flash droughts over China
740 during the recent global warming hiatus, *Sci. Rep.*, doi:10.1038/srep30571, 2016.

741 Wang, W., Wang, W. J., Li, J. S., Wu, H., Xu, C. and Liu, T.: The impact of sustained
742 drought on vegetation ecosystem in southwest China based on remote sensing, in
743 *Procedia Environmental Sciences.*, 2010.

744 Werner, A. T. and Cannon, A. J.: Hydrologic extremes - An intercomparison of multiple
745 gridded statistical downscaling methods, *Hydrol. Earth Syst. Sci.*,
746 doi:10.5194/hess-20-1483-2016, 2016.

747 Winston, H.A., Ruthi, L.J.: Evaluation of RADAP II severe-storm-detection algorithms.
748 *Bull. Am. Meteorol. Soc.*, 67(2), 145-150, doi.org/10.1175/1520-
749 0477(1986)067<0145:EORISS>2.0.CO;2 1986.

750 Wu, J., Chen, X., Yao, H., Liu, Z. and Zhang, D.: Hydrological Drought Instantaneous
751 Propagation Speed Based on the Variable Motion Relationship of Speed-Time

752 Process, *Water Resour. Res.*, doi:10.1029/2018WR023120, 2018.

753 Wu, X., Hao, Z., Hao, F. and Zhang, X.: Variations of compound precipitation and
754 temperature extremes in China during 1961–2014, *Sci. Total Environ.*, 663, 731–
755 737, doi:10.1016/j.scitotenv.2019.01.366, 2019.

756 Wu, X., Hao, Z., Zhang, X., Li, C. and Hao, F.: Evaluation of severity changes of
757 compound dry and hot events in China based on a multivariate multi-index
758 approach, *J. Hydrol.*, 583, 124580, doi:10.1016/j.jhydrol.2020.124580, 2020.

759 Xia, Y., Mocko, D. M., Wang, S., Pan, M., Kumar, S. V., and Peters-Lidard, C. D.:
760 Comprehensive evaluation of the variable infiltration capacity (VIC) model in the
761 North American Land Data Assimilation System. *Journal of Hydrometeorology*,
762 19(11), 1853-1879, 2018.

763 Xu, C., McDowell, N. G., Fisher, R. A., Wei, L., Sevanto, S., Christoffersen, B. O.,
764 Weng, E. and Middleton, R. S.: Increasing impacts of extreme droughts on
765 vegetation productivity under climate change, *Nat. Clim. Chang.*, 9(12), 948–953,
766 doi:10.1038/s41558-019-0630-6, 2019.

767 Xu, K., Yang, D., Yang, H., Li, Z., Qin, Y. and Shen, Y.: Spatio-temporal variation of
768 drought in China during 1961-2012: A climatic perspective, *J. Hydrol.*,
769 doi:10.1016/j.jhydrol.2014.09.047, 2015.

770 Yang, Y., Bai, L., Wang, B., Wu, J. and Fu, S.: Reliability of the global climate models
771 during 1961–1999 in arid and semiarid regions of China, *Sci. Total Environ.*,
772 doi:10.1016/j.scitotenv.2019.02.188, 2019.

773 Yeo, I. N. K. and Johnson, R. A.: A new family of power transformations to improve
774 normality or symmetry, *Biometrika*, 87(4), 954–959,
775 doi:10.1093/biomet/87.4.954, 2000.

776 Yu, H., Zhang, Q., Xu, C. Y., Du, J., Sun, P. and Hu, P.: Modified Palmer Drought

777 Severity Index: Model improvement and application, *Environ. Int.*, 130(January),
778 104951, doi:10.1016/j.envint.2019.104951, 2019.

779 Yuan, X., Wang, L., Wu, P., Ji, P., Sheffield, J. and Zhang, M.: Anthropogenic shift
780 towards higher risk of flash drought over China, *Nat. Commun.*,
781 doi:10.1038/s41467-019-12692-7, 2019.

782 Zhang, W. J., Lu, Q. F., Gao, Z. Q. and Peng, J.: Response of remotely sensed
783 normalized difference water deviation index to the 2006 drought of eastern
784 Sichuan Basin, *Sci. China, Ser. D Earth Sci.*, 51(5), 748–758, doi:10.1007/s11430-
785 008-0037-0, 2008.

786 Zhang, Y., You, Q., Chen, C. and Li, X.: Flash droughts in a typical humid and
787 subtropical basin: A case study in the Gan River Basin, China, *J. Hydrol.*, 551,
788 162–176, doi:10.1016/j.jhydrol.2017.05.044, 2017.

789 Zhang, Y., You, Q., Mao, G., Chen, C. and Ye, Z.: Short-term concurrent drought and
790 heatwave frequency with 1.5 and 2.0 °C global warming in humid subtropical
791 basins: a case study in the Gan River Basin, China, *Clim. Dyn.*, 52(7–8), 4621–
792 4641, doi:10.1007/s00382-018-4398-6, 2019.

793 Zhong, R., Chen, X., Lai, C., Wang, Z., Lian, Y., Yu, H. and Wu, X.: Drought
794 monitoring utility of satellite-based precipitation products across mainland China,
795 *J. Hydrol.*, 568(June 2018), 343–359, doi: 10.1016/j.jhydrol.2018.10.072, 2019a.

796 Zhong, R., Zhao, T., He, Y. and Chen, X.: Hydropower change of the water tower of
797 Asia in 21st century: A case of the Lancang River hydropower base, upper
798 Mekong, *Energy*, 179, 685–696, doi:10.1016/j.energy.2019.05.059, 2019b.

799 Zscheischler, J., Michalak, A. M., Schwalm, C., Mahecha, M. D. and Zeng, N.: Impact
800 of large-scale climate extremes on biospheric carbon fluxes: An intercomparison
801 based on MsTMIP data, *Global Biogeochem. Cycles*, 28(6), 585–600,

802 doi:10.1002/2014GB004826, 2014.

803 Zscheischler, J., Orth, R. and Seneviratne, S. I.: Bivariate return periods of temperature
804 and precipitation explain a large fraction of European crop yields, *Biogeosciences*,
805 doi:10.5194/bg-14-3309-2017, 2017a.

806 Zscheischler, J. and Seneviratne, S. I.: Dependence of drivers affects risks associated
807 with compound events, *Sci. Adv.*, 3(6), 1–11, doi:10.1126/sciadv.1700263, 2017b.

808 Zscheischler, J., Westra, S., Van Den Hurk, B. J. J. M., Seneviratne, S. I., Ward, P. J.,
809 Pitman, A., Aghakouchak, A., Bresch, D. N., Leonard, M., Wahl, T. and Zhang,
810 X.: Future climate risk from compound events, *Nat. Clim. Chang.*, 8(6), 469–477,
811 doi:10.1038/s41558-018-0156-3, 2018.

812 Zscheischler, J., Martius, O., Westra, S., Bevacqua, E. and Raymond, C.: A typology
813 of compound weather and climate events, *Nat. Rev. Earth Environ.*, doi:
814 <https://doi.org/10.1038/s43017-020-0060-z>, 2020.

815 Zhou, J., Wu, Z., He, H., Wang, F., Xu, Z., and Wu, X.: Regional assimilation of in situ
816 observed soil moisture into the VIC model considering spatial variability.
817 *Hydrological Sciences Journal*, 64(16), 1982-1996, 2019.

818

819

820

821

822

823

824

825

826

827 **Table**

828 Table 1 Categories of compound dry and hot conditions based on SCDHI.

Category	Dry-hot condition	SCDHI
Grade 0	Abnormal	(-0.80, -0.50]
Grade 1	Light	(-1.30, -0.80]
Grade 2	Moderate	(-1.60, -1.30]
Grade 3	Heavy	(-2.0, -1.60]
Grade 4	Extreme	≤ -2

829

830

831

832

833

834

835

836

837

838

839

840

841

842

843

844

845

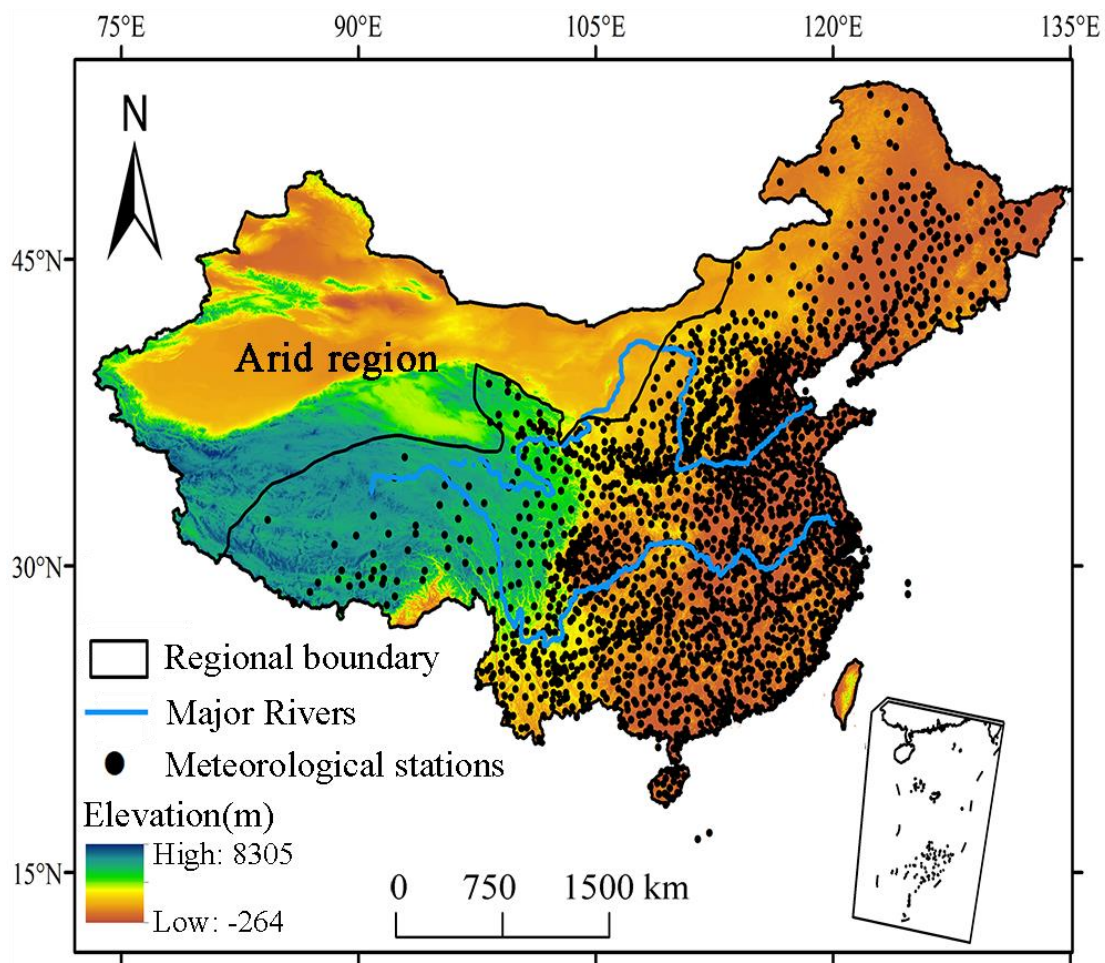
846

847

848

849

850 **Figure**



851

852 Figure 1 Geographical position of China and local of meteorological stations.

853

854

855

856

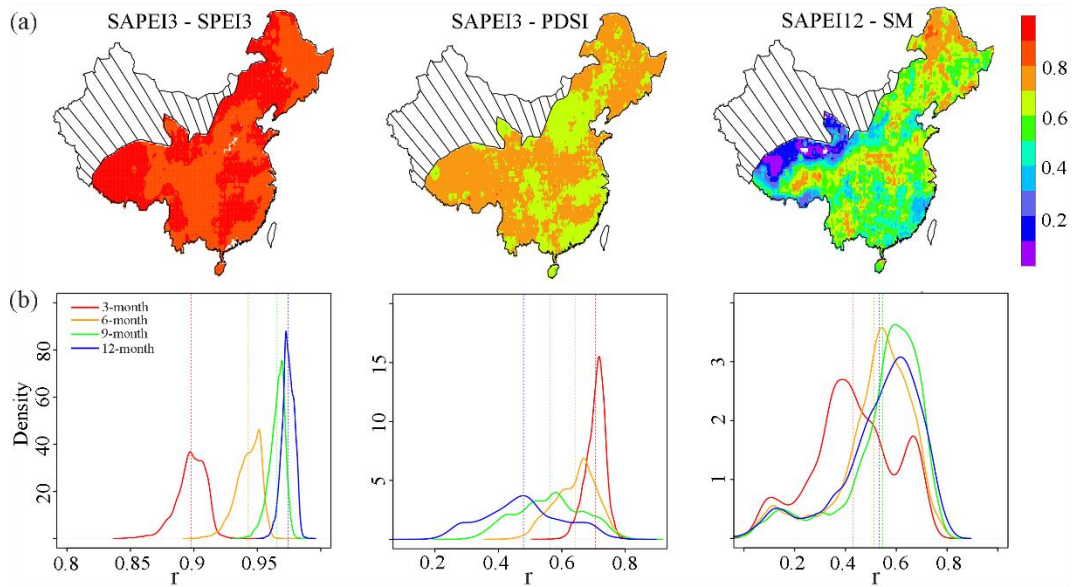
857

858

859

860

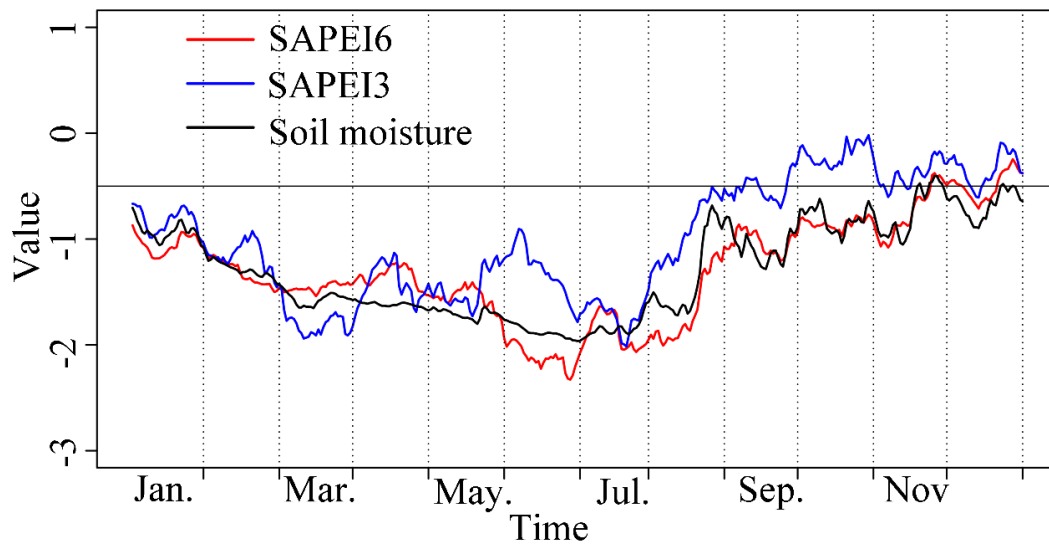
861



862

863 Figure 2 (a) The spatial pattern of the correlations between monthly SAPEI and
 864 SPEI/PDSI, and between daily SAPEI and soil moisture (SM), and (b) The density plot
 865 for the correlation coefficients between SAPEI and SPEI/PDSI/SM. The monthly
 866 SAPEI is computed by averaging the daily values in each month.

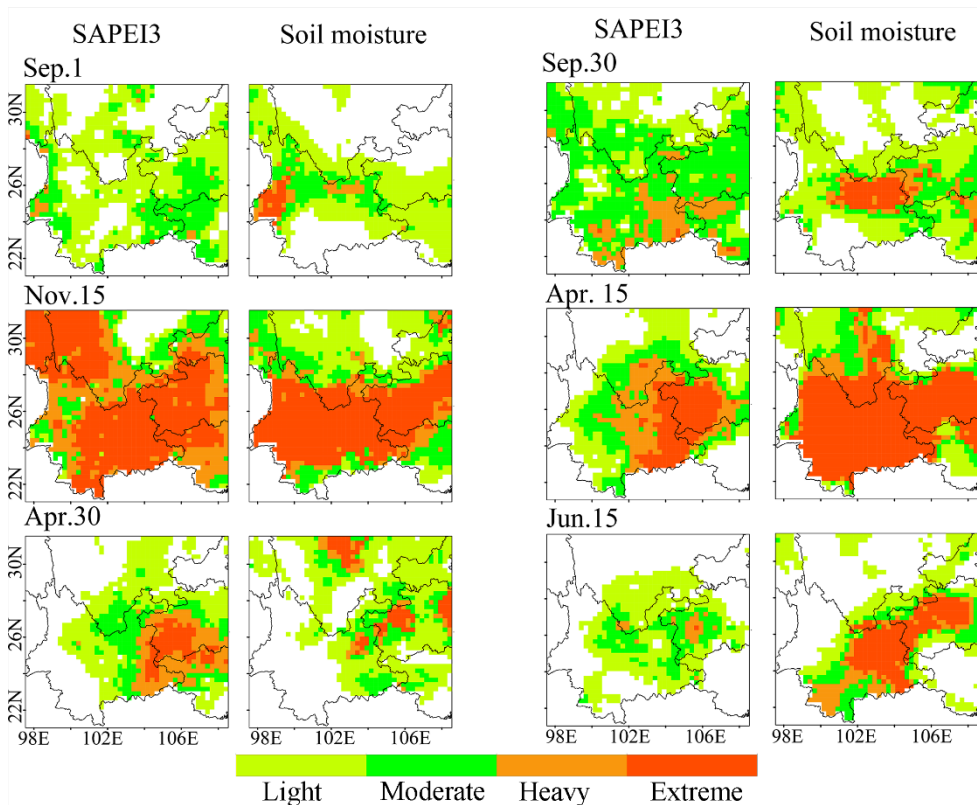
867



868

869 Figure 3 SAPEI and soil moisture series during the 2009/2010 drought event over the
 870 southwest China. The series were spatially average merged series. The value of solid
 871 black line is at -0.5, indicating the distinction between drought and non-drought.

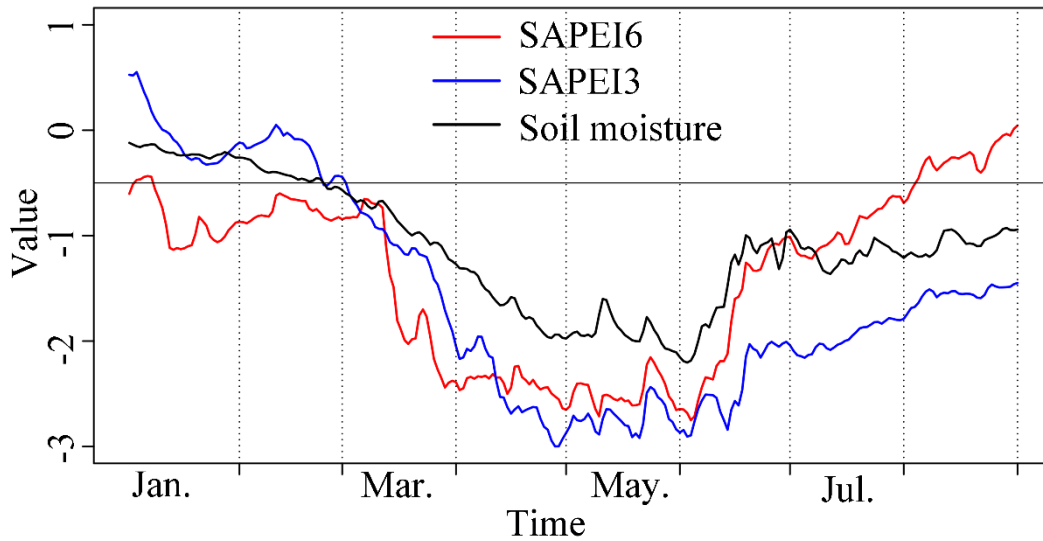
872



873

874 Figure 4 Daily evolutions of the 2009/2010 drought event over the southwest China

875 monitored by 3-month SAPEI and soil moisture.



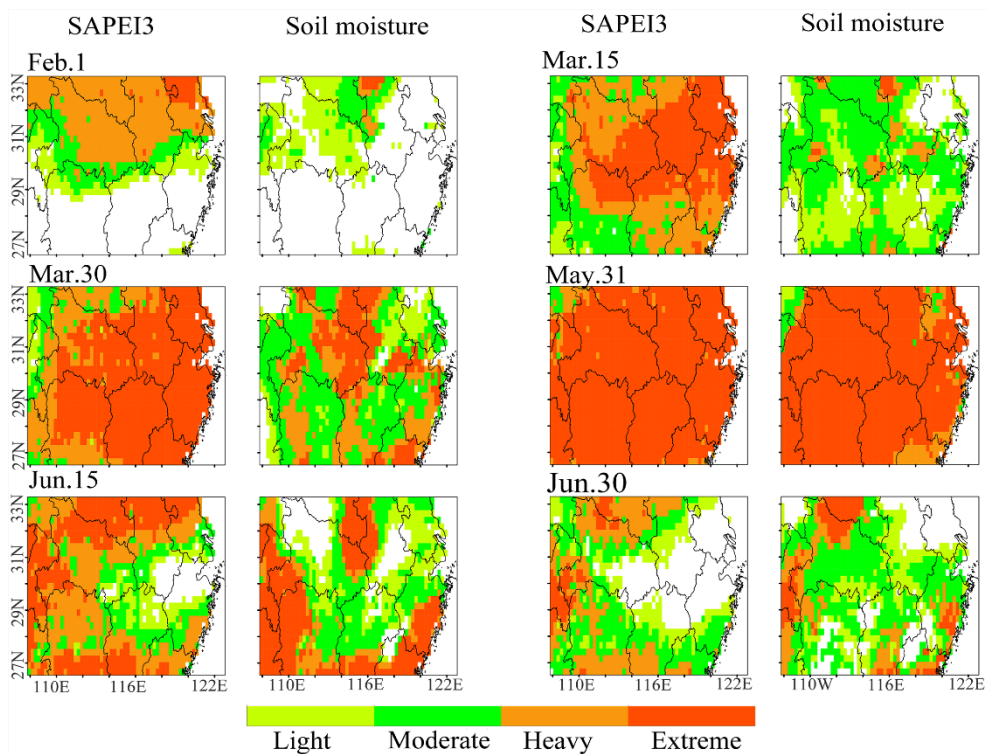
876

877 Figure 5 SAPEI (3- and 6-month) and soil moisture series during the 2011 drought

878 event over the middle and lower reaches of the Yangtze River. The series were spatially

879 average merged series. The value of solid black line is at -0.5, indicating the distinction

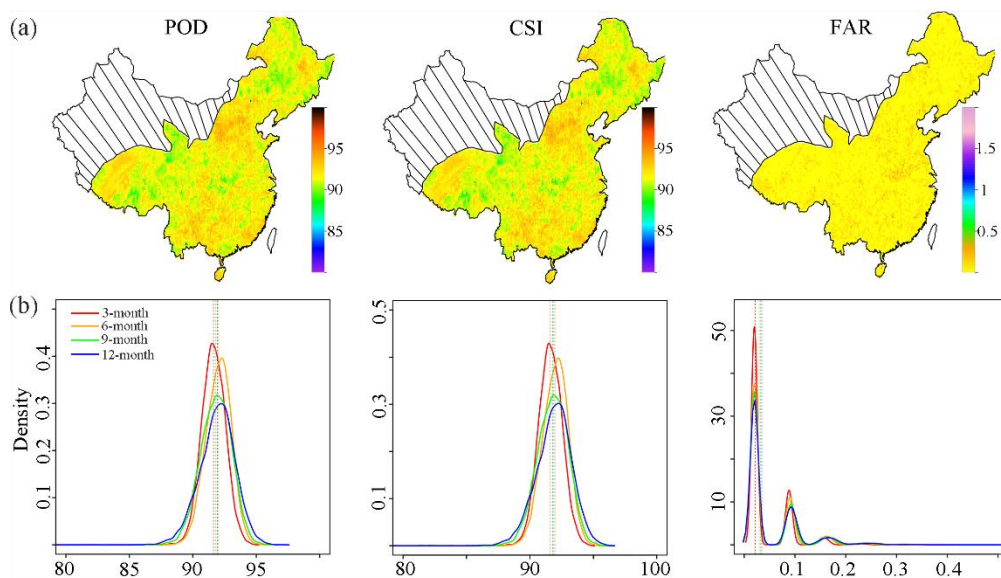
880 between drought and non-drought.



881

882 Figure 6 Daily evolutions of the 2011 drought event over the middle and lower reaches

883 of the Yangtze River monitored by 3-month SAPEI and soil moisture.



884

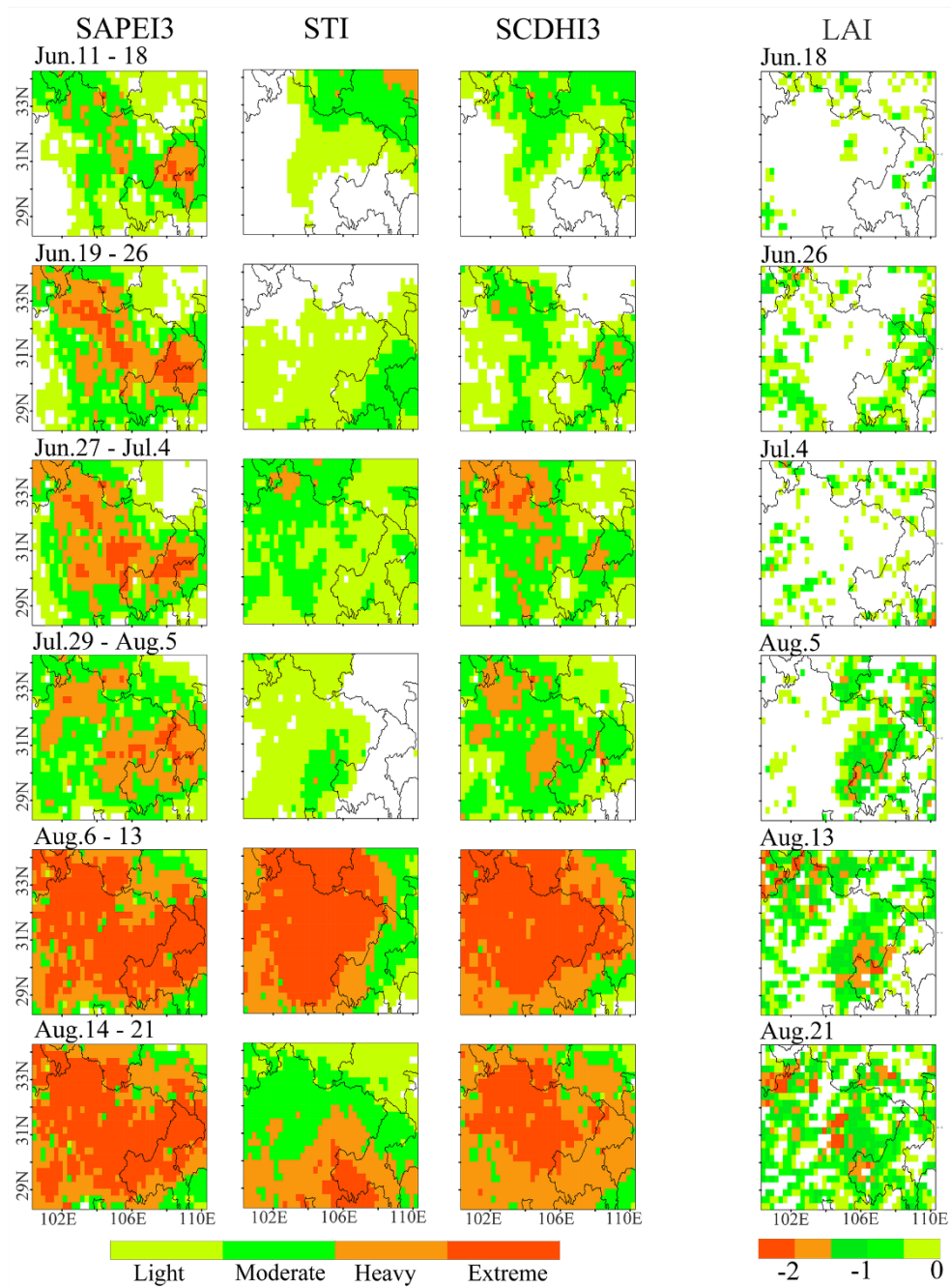
885 Figure 7 (a) The spatial pattern of probability of detection (POD, %), critical success

886 index (CSI, %), and false alarm ratio (FAR, %) for 3-month SCDHI from 1961 to 2018,

887 and (b) Density plot for POD, FAR, and CSI for 3-, 6-, 9-, 12-month SCDHI from 1961

888 to 2018.

889



890

891 Figure 8 The spatial evolutions of the compound dry and hot event over the Sichuan-
 892 Chongqing region in 2006 and its impact on vegetation.

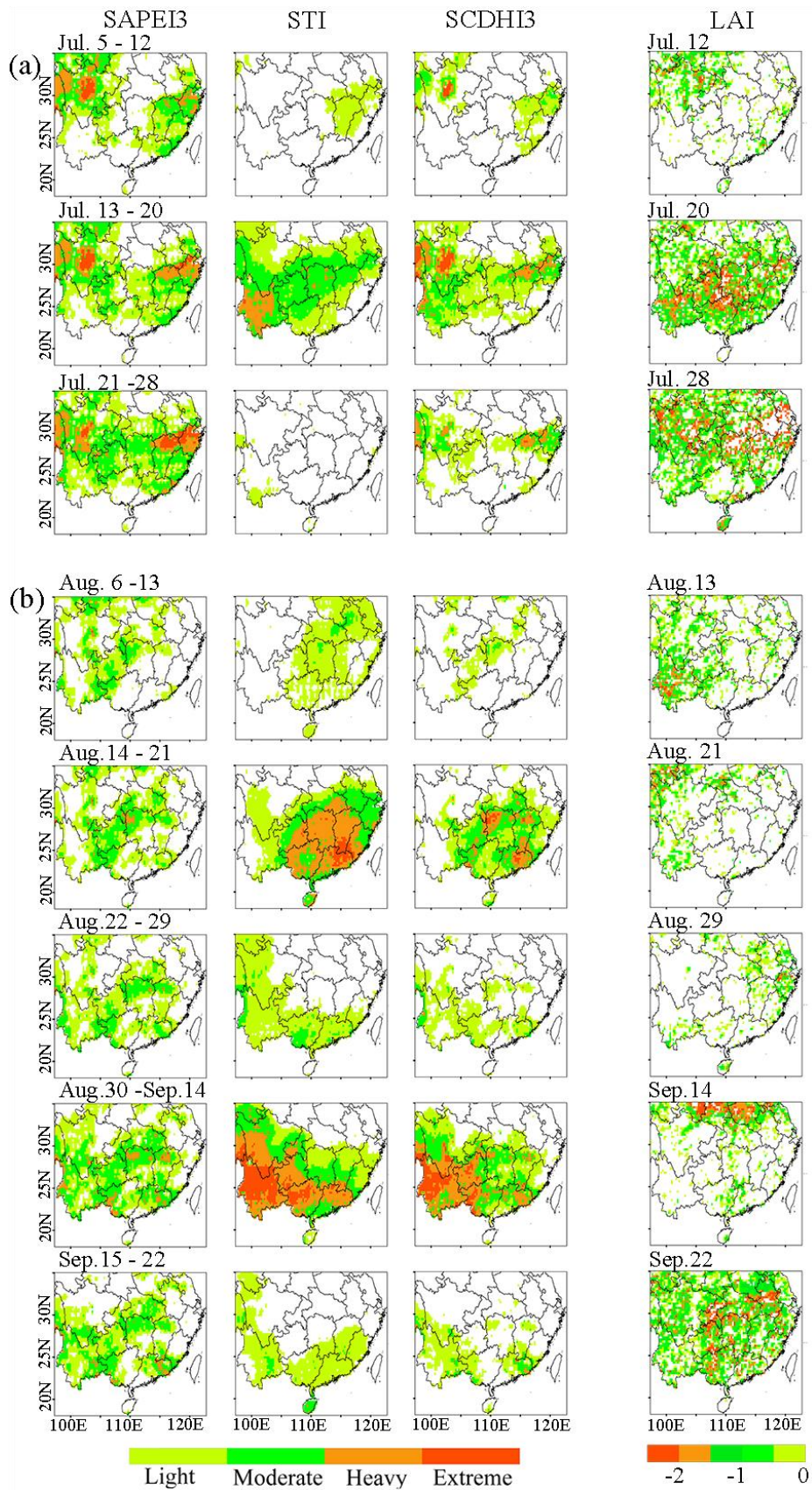
893

894

895

896

897

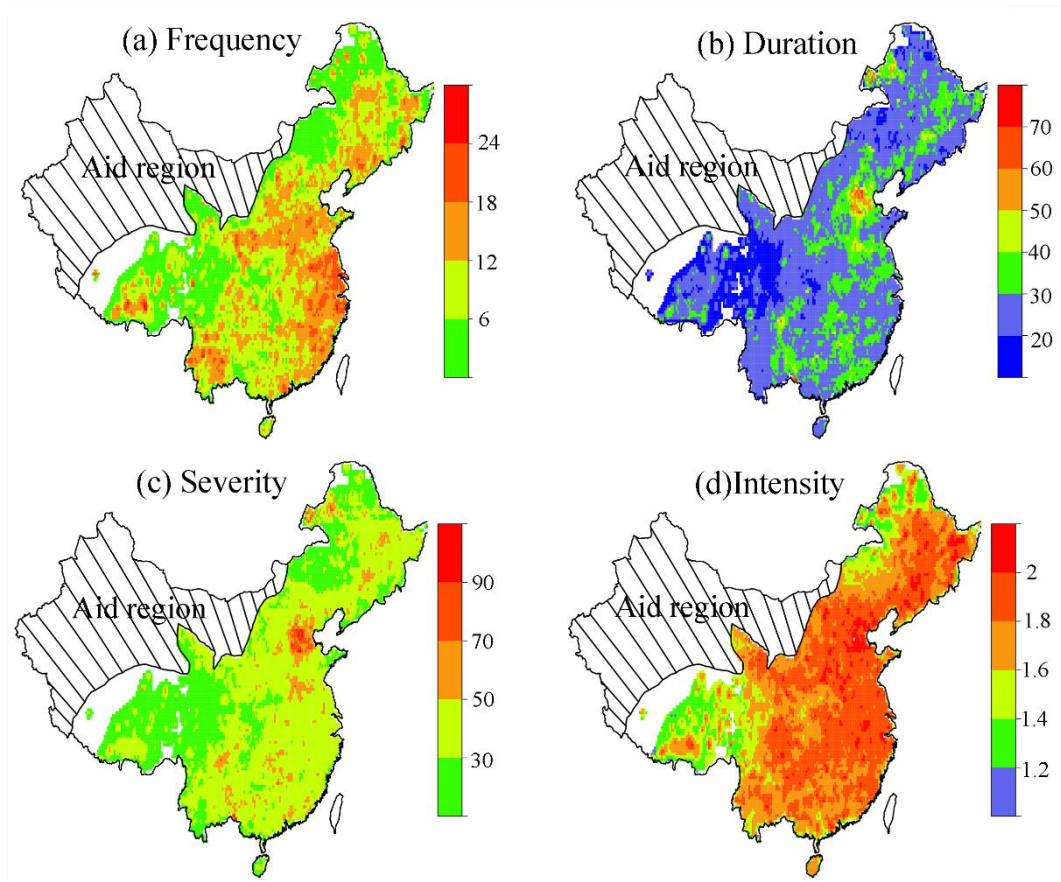


898

899 Figure 9 The spatial evolutions of the compound dry and hot event over the southern

900 China in 2009 and its impact on vegetation.

901



902

903 Figure 10 The spatial pattern of the characteristics of the compound dry and hot event
904 in China from 1961 to 2018.

905

906

907

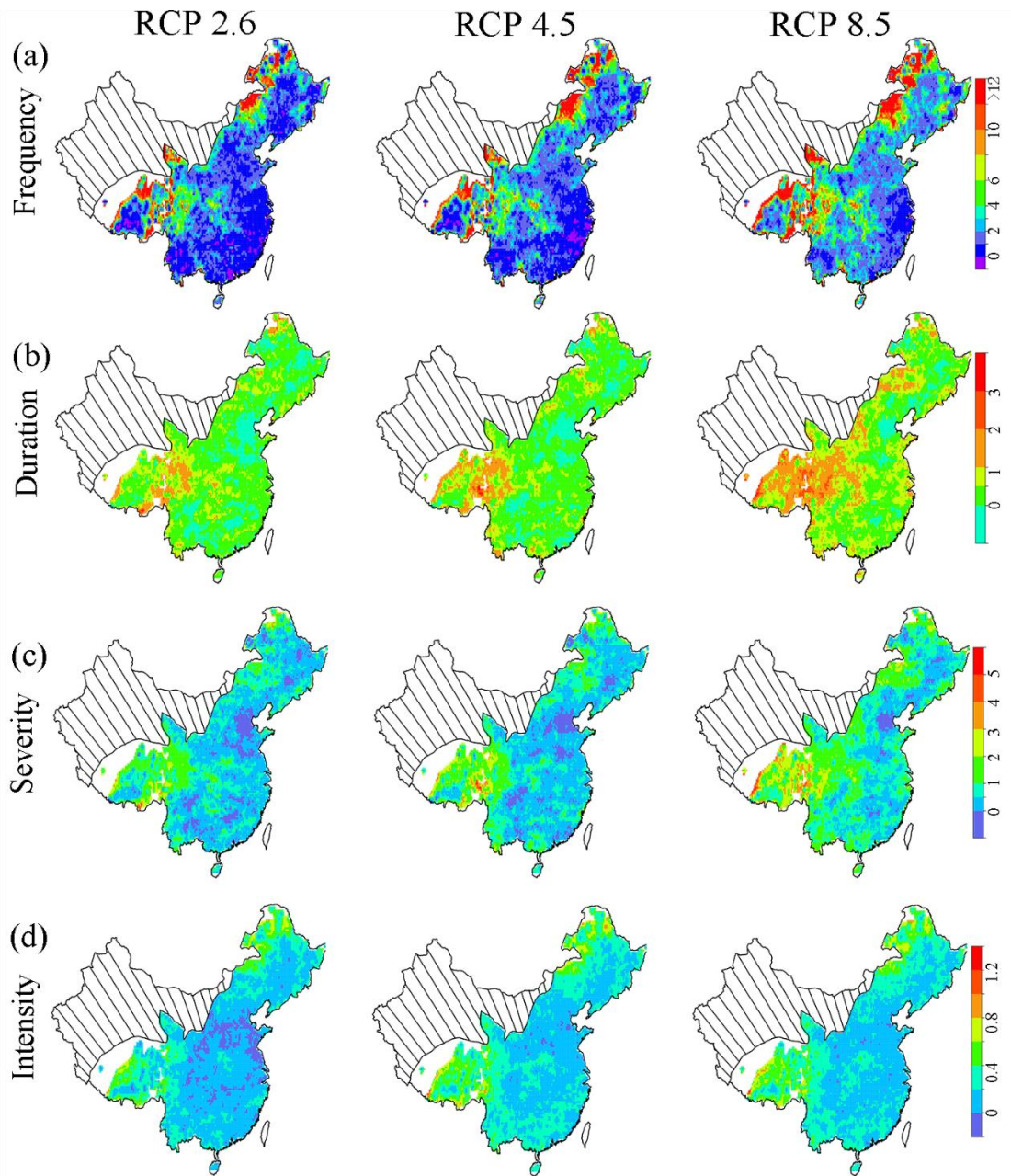
908

909

910

911

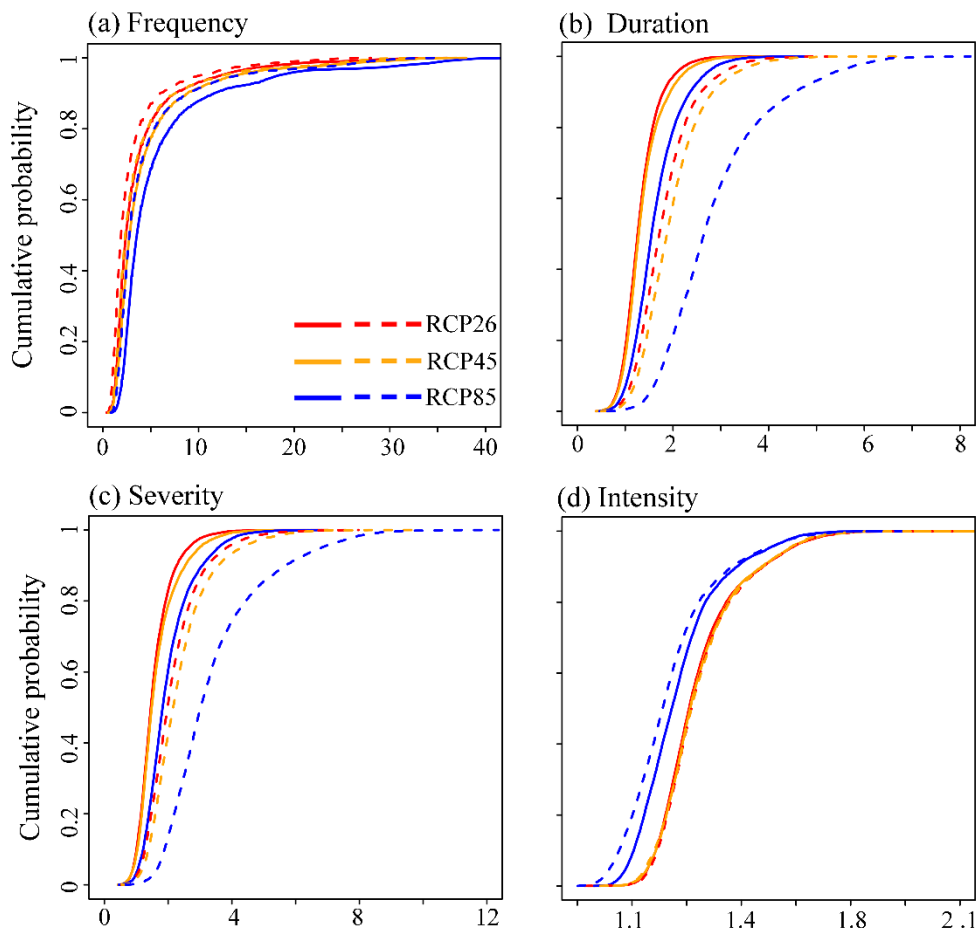
912



913

914 Figure 11 Future changes in characteristics of the compound dry and hot events under
 915 the RCP 2.6, RCP4.5 and RCP8.5 scenarios. The change values were the ratio of the
 916 future value to the reference values. Reference period: 1961-2018, and future period:
 917 2050-2100.

918



919

920 Figure 12 Cumulative probability of future changes (multiple) in of the compound dry-
 921 hot event characteristics. The dash lines indicate future characteristics changes only
 922 considered temperature change, while solid lines represent the future changes driven by
 923 all variable variation.